(14) Kim, J. J.; Beardslee, R. A.; Phillips, D. T.; Offen, H. W. J. Chem. Phys. 1969, 51, 2761.
(15) Scott, R. L. J. Chem. Phys. 1949, 17, 279.
(16) de Gennes, P.-G. J. Polym. Sci., Polym. Phys. Ed. 1978, 16, 1883.
(17) Burrell, H. Interchem. Rev. 1955, 14, 3, 31.
(18) Gardon, J. L. In "Encyclopedia of Polymer Science and Technology"; Mark, H. F. et al., Eds.; Interscience: New York, 1965; Vol. 3, pp 833–862.
(19) Small, P. A. J. Appl. Chem. 1953, 3, 71.
(20) In ref 7, Chapter 9.
(21) In ref 7, Chapter 13.

Spectrum of Light Quasielastically Scattered from Solutions of Very Long Rods at Dilute and Semidilute Regimes

Tadakazu Maeda and Satoru Fujime*

Mitsubishi-Kasei Institute of Life Sciences, Machida, Tokyo 194, Japan.
Received June 8, 1983

ABSTRACT: A theoretical model is considered for the effect of anisotropic translational diffusion on the polarized field correlation function $G^1(\tau)$ of light quasielastically scattered from solutions of very long rods. Without solving a coupled translational/rotational diffusion equation, an expression for the first cumulant of $G^1(\tau)$ is derived, which is exactly the same as a recent one by a different approach. The Green function to the coupled diffusion equation in a dilute regime is obtained by two approximations. Since the Green function is characterized only by the sideways (D_1) and lengthways (D_3) translational and the rotational (Θ) diffusion constants, it is applicable to the case of semidilute solutions of rods after simple replacement of these constants with those suitable for a semidilute regime. Using this Green function, we formulate an expression of $G^1(\tau)$ for solutions of very long rods at arbitrary values of $\mu^2 = (D_3 - D_1)K^2/\Theta$ or of its version at a semidilute regime, where K is the length of the scattering vector. Some of simulated $G^1(\tau)$ are presented in order to estimate the accuracy of approximations and to visualize the theory. The present result includes the previous ones for relatively short rod lengths. Our model is easily extendable to the case of a solution of slightly bendable rods. A brief discussion on this context will also be given.

Introduction

Quasielastic scattering of laser light has been extensively applied to dynamic studies of macromolecules in solution. We have been interested in the dynamics of very long and semiflexible (or slightly bendable) filaments in solution. Such filaments include muscle F-actin and its complexes with other muscle proteins,[1-7] bacterial flagella,[8] various kinds of rodlike viruses,[9,10] microtubule,[11] and muscle thin[10] and thick[12] filaments. For example, the thin filament of skeletal muscle is 1 μm in length (L) and 5–8 nm in diameter (d).

To interpret experimental spectra (time correlation functions or power spectra of scattered light) from solutions of such long and semiflexible filaments, theoretical models for rigid rods undergoing translational and rotational Brownian motions are usually applied as the first-order approximation. Because a long rod undergoes anisotropic translation, a coupling between translational and rotational modes of diffusive motions is expected. This effect was once studied with special reference to tobacco mosaic virus (TMV).[13,14] In this case, however, experimental results excluded importance of the coupling effect.[14] And no further study has been made of this effect either theoretically or experimentally for a long time. But, if one wants to study very long rods, one has to take account of the coupling effect. Recently, a multiple time scale asymptotic technique was applied to this problem and experimental data on TMV were reanalyzed, which again gave small anisotropy.[15] More recently, an expression for the first cumulant of the polarized-light field correlation function for a long, thin rod was derived on the basis of a velocity autocorrelation function technique, and experimental data on TMV were analyzed, which gave quite large anisotropy, as large as the theoretically expected one.[16]

In the case of semidilute solutions, one has to take account of an effect of entanglements of long rods. Let c be the number of rods in unit volume. Then, one has to distinguish the two cases, $cL^3 \ll 1$ (dilute regime) and $L/d \gg cL^3 \gg 1$ (semidilute regime). In the case of muscle thin filaments, for example, 1 mg/mL in protein concentration corresponds to $cL^3 = 40$. Doi and Edwards considered the light-scattering spectra from a semidilute solution of relatively short rods.[17] Their model has been tested with (semi-) quantitative success by measurements of, for example, the Kerr effect (long viruses[18a] and a synthetic polymer[26]) and light scattering (long virus[18b] and a synthetic polymer[19]). As far as the light-scattering problem is concerned, the Doi–Edwards model corresponds to the extreme case of anisotropic translation of a rod. In the framework of their model, we can develop a unified theory of light scattering from solutions of long rods at dilute and semidilute regimes. The theories so far proposed for the effect of anisotropic translation on light-scattering spectrum are valid only for solutions of relatively short rods. We will consider a case of very long rods. Under the assumptions we adopted, our theory given below includes the previous ones for shorter rod lengths.

Even if a rod seems (or is believed) to be rigid, it might be semiflexible when it is very long. On electron micrographs of all the above-mentioned filaments, one surely observes *gradually curved images*. Thus, one has to take account of the effect of filament flexibility on the spectra. We have published a paper on the effect of filament flexibility on light-scattering spectra,[20] where neither the coupling nor the entanglement effect was considered.

As the first step to improve our old model,[20] we discuss in this paper a theoretical model for very long rods undergoing anisotropic translation as well as rotation at dilute and semidilute regimes. Because the main aim of this paper is to show gross features characteristic of light-scattering spectra of solutions of very long rods, a very simple model will be adopted and no sophisticated interaction will be considered. The outline of a part of this study has been published.[21]

Model

The polarizability α_3 parallel to the long axis of the rod

0024-9297/84/2217-1157$01.50/0

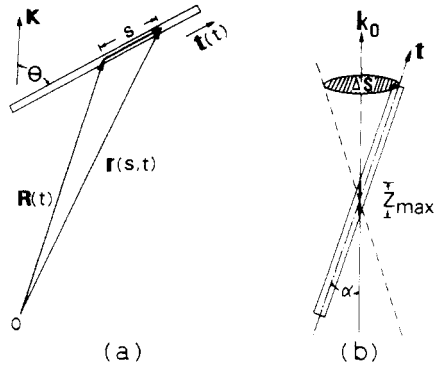

Figure 1. Illustrations of geometrical relationships. (a) The relationship between various vectors defining the position vector $\vec{r}(s,t)$ of the line element ds (for details, see text). (b) An illustration showing the relationship between the optical path length Z and the orientation of a rod (for details, see text).

is not equal to the perpendicular components α_1 ($=\alpha_2$). However, as far as the polarized light-scattering spectrum is concerned, we can assume a relationship $[(\alpha_1 + \alpha_2 + \alpha_3)/3]^2 \gg (\alpha_3 - \alpha_1)^2$. Under this assumption, we can express various mathematical relations in terms of the Legendre polynomials $P_n(\theta)$ instead of the spherical harmonics $Y_{nm}(\theta,\phi)$. This makes our treatments very simple. The unnormalized polarized field correlation function $G^1(\tau)$ of scattered light in the optically isotropic case is given by

$$G^1(\tau) = (1/L^2)\int\int_{-L/2}^{L/2} J(s,s',\tau)\, ds\, ds' \quad (1a)$$

$$J(s,s',\tau) = \langle \exp[i\vec{K}\cdot\{\vec{r}(s,t) - \vec{r}(s',t')\}]\rangle \quad (1b)$$

where $\tau \equiv |t - t'|$, $\vec{K}$ is the momentum-transfer vector, and $\vec{r}(s,t)$ is the position vector of the line element ds at s from the center of the rod:

$$\vec{r}(s,t) = \vec{R}(t) + s\vec{t}(t) \quad (2)$$

Here $\vec{R}(t)$ is the position vector of the center-of-mass of the rod and $\vec{t}(t)$ is the unit vector parallel to the long axis of the rod (Figure 1a). Equation 1b includes only the geometrical phase relationship (or the path-difference relationship) of scattered rays. It does not include the wave-optical one. In a case of a long *and not very thin* rod, we have to consider the so-called Rayleigh–Debye condition

$$(4\pi/\lambda)(n - n_0)Z \ll 1 \quad (3)$$

where λ is the wavelength of light in vacuum, n and n_0 are the refractive indices of solute and solvent, respectively, and Z is the characteristic dimension of a scatterer. For $(n - n_0) \simeq 0.3$ (a protein rod in aqueous solution) and $\lambda \simeq 500$ nm, eq 3 gives $Z \ll 140$ nm. Now, let α be the angle between the vector $\vec{t}$ and the incident wave vector $\vec{k}_0$ (or the scattered wave vector $\vec{k}_s$). When the tip of the rod lies within an area ΔS on the surface of radius $L/2$ (Figure 1b), the length Z (shown by the thick line in Figure 1b) violates eq 3. The probability P of finding the tip of the rod in ΔS is given by $P = \Delta S/S$, with $S = 4\pi(L/2)^2$. For small α (i.e., small d), we have $\sin\alpha \simeq d/Z_{max}$ and $\Delta S \simeq \pi(L/2)^2 \sin^2\alpha \simeq \pi(L/2)^2(d/Z_{max})^2$ and hence $P \simeq (d/Z_{max})^2$, where Z_{max} is the maximum value of Z which satisfies eq 3. For a very thin rod, violation of eq 3 is negligible irrespective of its length L ($\gg d$). On the other hand, for practical values of d = 5–20 nm (rodlike macromolecules composed of protein protomers such as rodlike viruses, muscle filaments, various kinds of bacterial flagella, etc.), the value of P is not negligibly small irrespective of their length L ($\gg d$). For most of the scattering angles, our model is not quantitatively correct for d values of our interest. However, as shown below, the intensity at $KL \gg 1$ of scattered light from solutions of rods is exclusively contributed from those whose $\vec{t}$ is perpendicular to $\vec{K}$ (cf. Figure 2a). In such a situation, we have an average Z value of $\sim d$ at the scattering angle of 180°. Our model would be quantitatively correct for the cases of large KL *and* large K (backward scattering), where our discussion will be concentrated. For large L *and* small K values, where our model violates eq 3 mainly due to a finite thickness of the rod, our results given below should be regarded as qualitative ones. However, characteristic features of our model would play a role of a guiding principle in the analysis of experimental data of any pair of L and K values.

(1) At Dilute Regime. The orientation of the rod, $\vec{t}(t)$ in eq 2, is specified by the polar coordinates θ and ϕ, and the polar axis is taken to be parallel to the vector $\vec{K}$ (Figure 1a). Then we have

$$J(s,s',\tau) = \int_V\int\int_\Omega e^{iK(s\xi - s'\xi')} e^{(i\vec{K}\cdot(\vec{R}-\vec{R}')} G(\vec{R} - \vec{R}',\vec{t},\vec{t}';\tau) P_0(\vec{R}')P_0(\vec{t}')\, d(\vec{R} - \vec{R}')\, d\vec{R}'\, d\vec{t}\, d\vec{t}' \quad (4)$$

where $P_0(\vec{R}') = 1/V$ is the uniform distribution function of the initial value $\vec{R}' = \vec{R}(t')$ in volume V, $P_0(\vec{t}') = 1/\Omega = (1/2)(1/2\pi)$ is the uniform distribution function of the initial values $\theta' = \theta(t')$ and $\phi' = \phi(t')$, $\xi = \cos\theta$, and G is the conditional probability that, if a rod is found at $\vec{R}'$ with orientation $\vec{t}'$ at time t', it will be found at $\vec{R}$ with orientation $\vec{t}$ at a later time t, or mathematically the Green function to the diffusion equation in the laboratory-fixed coordinate system

$$[\partial/\partial\tau - D_3(\vec{t}\cdot\partial/\partial\vec{R})^2 - D_1\{\partial^2/\partial R^2 - (\vec{t}\cdot\partial/\partial\vec{R})^2\} - \Theta\nabla_{\theta\phi}^2]G = \delta(\vec{R} - \vec{R}')\delta(\vec{t} - \vec{t}')\delta(\tau) \quad (5)$$

where $\nabla_{\theta\phi}^2$ is the Laplace operator with respect to θ and ϕ and D_1, D_3, and Θ are, respectively, the sideways and lengthways translational and the rotational diffusion constants. Let $G_K(\xi,\xi';\tau)$ be the Fourier space transform of $G(\vec{R} - \vec{R}',\vec{t},\vec{t}';\tau)$, and define

$$D = (2D_1 + D_3)/3 \quad \text{(average diffusion constant)} \quad (6a)$$

$$\mu^2 = (D_3 - D_1)K^2/\Theta \quad \text{(coupling constant)} \quad (6b)$$

$$G_K(\xi,\xi';\tau) = G_D(\tau)g_K(\xi,\xi';\tau) \quad (6c)$$

$$G_D(\tau) = \exp[-\{D - \tfrac{1}{3}(D_3 - D_1)\}K^2\tau] \equiv \exp(-D_1K^2\tau) \quad (6d)$$

where, and below, we intentionally use the expression $[D - {}^1/_3(D_3 - D_1)]$ instead of D_1 in order to explicitly show anisotropy $D_3 \neq D_1$. Integration of eq 4 over $\vec{R} - \vec{R}'$, $\vec{R}'$, ϕ, and ϕ' gives

$$J(s,s',\tau) = G_D(\tau)J_\theta(s,s',\tau) \quad (7)$$

$$J_\theta(s,s',\tau) = \tfrac{1}{2}\int\int_{-1}^{1} e^{iK(s\xi - s'\xi')} g_K(\xi,\xi';\tau)\, d\xi\, d\xi' \quad (8)$$

where $g_K(\xi,\xi';\tau)$ satisfies (cf. eq 5)

$$[\partial/\partial\tau - \Theta(\nabla_\xi^2 - \mu^2\xi^2)]g_K(\xi,\xi';\tau) = \delta(\xi - \xi')\delta(\tau) \quad (9)$$

In the long-rod limit $L/d \gg 1$, we have $D_3 = 2D_1$ and $\Theta = 12D_1/L^2$, and hence $\mu^2 = (KL)^2/12$. Putting

$$g_K(\xi,\xi';\tau) = \sum_n A_n(K,\xi',\tau)P_n(\xi) \quad (10)$$

where $P_n(\xi)$ is the Legendre polynomial, we have (see Appendix A)

$$A_l(K,\xi',0) = \frac{2l+1}{2}P_l(\xi') \quad (11)$$

$$\partial A_n/\partial(\Theta\tau) = -[n(n+1) + \mu^2L_0(n)]A_n - \mu^2L_1(n)A_{n-2} - \mu^2L_2(n)A_{n+2} \quad (12)$$

where

$$L_0(n) = \frac{2n^2 + 2n - 1}{(2n - 1)(2n + 3)}$$

$$L_1(n) = \frac{n(n - 1)}{(2n - 1)(2n - 3)}$$

$$L_2(n) = \frac{(n + 1)(n + 2)}{(2n + 3)(2n + 5)} \quad (13)$$

By putting $A_{N+2} = A_{N+4} = ... = 0$ for an appropriate even number N and defining

$$\mathbf{A} = (A_0, A_2, ..., A_N)^T \quad (14)$$

where T stands for transposition, and

$$\mathbf{M} = \{a_{n,n'}\} \quad (15)$$

where $a_{n,n} = n(n + 1) + \mu^2 L_0(n)$, $a_{n,n-2} = \mu^2 L_1(n)$, $a_{n,n+2} = \mu^2 L_2(n)$, and $a_{n,n'} = 0$ for $n' \neq n, n \pm 2$, eq 12 can be written in a matrix form as[14]

$$\partial \mathbf{A}(K,\xi',\tau)/\partial(\Theta\tau) = -\mathbf{M}\mathbf{A}(K,\xi',\tau) \quad (16)$$

Since there is no coupling between A_n and A_{n+1} and since we need A_n's for even n only, we construct the matrix $\mathbf{M}$ in a way that the element $a_{n,n'}$ is placed at $(n/2, n'/2)$ including the (0, 0) element (ref 22).

Using the matrix $\mathbf{U}$ which satisfies

$$\mathbf{MU} = \mathbf{U}\Lambda \quad (17)$$

where Λ is a diagonal matrix, we have the solution of eq 16 as

$$\mathbf{A}(K,\xi',\tau) = [\mathbf{U} \exp(-\Lambda\Theta\tau)\mathbf{U}^{-1}]\mathbf{A}(K,\xi',0) \quad (18)$$

or in the component representation as[23]

$$A_n(K,\xi',\tau) = \sum_l [\mathbf{U} \exp(-\Lambda\Theta\tau)\mathbf{U}^{-1}]_{nl} A_l(K,\xi',0) \quad (19a)$$

$$= \sum_p \sum_l \exp(-\lambda_p\Theta\tau) U_p(n) U_p^*(l) A_l(K,\xi',0) \quad (19b)$$

where $\mathbf{U}^{-1}$ is the inverse matrix of $\mathbf{U}$, $U_p(n)$ is the nth element of the pth column (or the n, p element) of $\mathbf{U}$, $U_p^*(l)$ is the lth element of the pth line (or the p, l element) of $\mathbf{U}^{-1}$, and λ_p is the p, p element of Λ. Then, we have from eq 10, 11, and 19

$$g_K^{\mu}(\xi,\xi';\tau) = \sum_n \sum_l \frac{2l + 1}{2} [\mathbf{U} \exp(-\Lambda\Theta\tau)\mathbf{U}^{-1}]_{nl} P_n(\xi) P_l(\xi') \quad (20a)$$

$$= \sum_n \sum_p \sum_l \frac{2l + 1}{2} \exp(-\lambda_p\Theta\tau) U_p(n) U_p^*(l) P_n(\xi) P_l(\xi') \quad (20b)$$

The superscript μ attached to $g_K(\xi,\xi';\tau)$ means that eq 20 is valid for any value of μ provided that N in eq 14 is properly chosen (see Discussion).

For $\mu \simeq 0$ ($D_3 - D_1 \ll 1$ and/or $KL \lesssim 1$), eq 20 is reduced to

$$g_K^0(\xi,\xi';\tau) = \sum_n \frac{2n + 1}{2} \exp[-n(n + 1)\Theta\tau] P_n(\xi) P_n(\xi') \quad (21)$$

where the superscript 0 attached to $g_K(\xi,\xi';\tau)$ means $\mu \simeq 0$.

For $\mu \gg 1$ ($D_3 \neq D_1$ and $KL \gg 1$), we have an approximate but very simple form of $g_K(\xi,\xi';\tau)$. In terms of the new variable $\zeta = \mu^{1/2}\xi$, the "Hamiltonian" $H = -\nabla_\xi^2 + \mu^2\xi^2$ is written as $H = \mu[-\partial^2/\partial\zeta^2 + (1/\mu)(\partial/\partial\zeta)\zeta^2(\partial/\partial\zeta) + \zeta^2]$. In the limit of $\mu \to \infty$, this Hamiltonian becomes exactly that of a harmonic oscillator, so that the Green function can be obtained by using eigenfunctions and eigenvalues for the harmonic oscillator:[17]

$$g_K(\zeta,\zeta';\tau) = \sum_n \frac{1}{\pi^{1/2} 2^n n!} e^{-(\zeta^2+\zeta'^2)/2} H_n(\zeta) H_n(\zeta') e^{-(2n+1)\mu\Theta\tau} \quad (22)$$

where $H_n(\zeta)$ is the Hermite polynomial. Using an integral expression for $H_n(\zeta)$, we can carry out the summation over n exactly. For $\mu \gg 1$ (at least $\mu^{1/2} \geq 10$ because $\exp(-\zeta^2/2)H_n(\zeta)$ has appreciable values in a range $|\zeta| \leq 7$), an approximate form of $g_K(\xi,\xi';\tau)$ can be obtained:[17]

$$g_K^{\gg}(\xi,\xi';\tau) = \left[\frac{\mu}{2\pi \sinh(2\mu\Theta\tau)}\right]^{1/2} \times \exp\left[-\mu \frac{(\xi^2 + \xi'^2)\cosh(2\mu\Theta\tau) - 2\xi\xi'}{2 \sinh(2\mu\Theta\tau)}\right] \quad (\mu \gg 1) \quad (23)$$

where the superscript $\gg$ attached to $g_K(\xi,\xi';\tau)$ means $\mu \gg 1$.

From eq 1, 7, 8, 20, and A3 in Appendix A, we obtain

$$G^1(\tau) = G_D(\tau) \sum_n \sum_l (2l + 1)[\mathbf{U} \exp(-\Lambda\Theta\tau)\mathbf{U}^{-1}]_{nl} (i)^n (-i)^l b_n(k) b_l(k) \quad (24a)$$

$$= G_D(\tau) \sum_n \sum_p \sum_l (2l + 1) U_p(n) U_p^*(l) (i)^n (-i)^l b_n(k) b_l(k) e^{-\lambda_p\Theta\tau} \quad (24b)$$

where summation is carried out over even n and l, $G_D(\tau)$ is given by eq 6d and for $k \equiv KL/2$

$$b_n(k) = (1/k) \int_0^k j_n(z)\, dz \quad (\text{even } n) \quad (25a)$$

$$b_n(k) = 0 \quad (\text{odd } n) \quad (25b)$$

Since $\mathbf{UU}^{-1} = \mathbf{E}$, we have $G^1(0) = \sum_n (2n + 1) b_n(k)^2$. For $\mu = 0$, eq 24 is reduced to

$$G^1(\tau) = \sum_n (2n + 1) b_n(k)^2 e^{-[DK^2 + n(n+1)\Theta]\tau} \quad (\mu = 0) \quad (26)$$

which just corresponds to the Pecora formula for rods.[24]

By use of identity relations $\xi^2 + \xi'^2 = [(\xi + \xi')^2 + (\xi - \xi')^2]/2$ and $2\xi\xi' = [(\xi + \xi')^2 - (\xi - \xi')^2]/2$, eq 23 can be written as

$$g_K^{\gg}(\xi,\xi';\tau) = \left[\frac{\mu}{2\pi \sinh(2\mu\Theta\tau)}\right]^{1/2} \exp[-(\mu/4) \times (\xi - \xi')^2/\tanh(\mu\Theta\tau)] \exp[-(\mu/4)(\xi + \xi')^2 \tanh(\mu\Theta\tau)] \quad (27)$$

Then, we have for $\mu \gg 1$ (see Appendix A)

$$G^1(\tau) = G_D(\tau) \operatorname{sech}(\mu\Theta\tau) \frac{2}{(KL)^2} \int_0^{KL} dy \int_0^1 y j_0(y\eta) \times \exp\left[-\kappa^2 \left\{(\mu\eta)^2 + \frac{(KL - y)^2}{4}\right\}\right] d\eta \quad (\mu \gg 1) \quad (28)$$

where $\kappa^2 = \tanh(\mu\Theta\tau)/\mu$.

Without the numerical computation of $G^1(\tau)$ given by eq 24, the time behavior of the correlation function cannot be known. However, the first cumulant $\bar{\Gamma}$ of $G^1(\tau)$ can easily be known (see Appendix B):

$$\bar{\Gamma}/K^2 = [D - \tfrac{1}{3}(D_3 - D_1)] + (L^2/12)\Theta f_1(k) + (D_3 - D_1) f_2(k) \quad (29)$$

where both $f_1(k)$ and $f_2(k)$ are functions depending only on $k \equiv KL/2$. Since $f_1(k) \to 0$ and $f_2(k) \to {}^1/_3$ as $k \to 0$, and $f_1(k) \to 1$ and $f_2(k) \to 0$ as $k \to \infty$ (see Appendix C),

we have the limiting values of

$$\bar{\Gamma}/K^2 \to D \qquad (k \ll 1) \tag{30a}$$

$$\bar{\Gamma}/K^2 \to [D - \tfrac{1}{3}(D_3 - D_1)] + (L^2/12)\Theta \qquad (k \gg 1) \tag{30b}$$

(2) At Semidilute Regime. In a case where there are many rods in volume L^3, the rotational motion of each rod will be severely restricted as well as the sideways translation, whereas the lengthways translation is almost free. Doi and Edwards treated the problem as follows.[17] Consider a model situation: If the rod which has been preventing a test rod from rotating (and sideways translating), diffuses a distance of order L, the constraint imposed by the rod is released and the test rod can rotate by a small amount of order a_c/L (and translating sideways by a small amount of order a_c) during a time $t_0 \simeq L^2/D_3$. This model is equivalent to the case where we assume a "cage" which confines the test rod. The cage has a radius a_c and a lifetime $\tau_{cage} = t_0$. It is possible to imagine the free rotation of the test rod in the cage for a very short time. However, this will have no appreciable effect on $G^1(\tau)$ as discussed in Appendix D. So, we assume

$$\bar{D}_1 = \bar{D}_2 \simeq a_c^2/t_0 \simeq \beta D_1 \qquad \bar{D}_3 = D_3 \tag{31a}$$

$$\bar{\Theta} \simeq (a_c/L)^2/t_0 \simeq \beta\Theta \tag{31b}$$

where $\beta = (a_c/L)^2$. Putting

$$\bar{\mu}^2 = (\bar{D}_3 - \bar{D}_1)K^2/\bar{\Theta} \tag{32a}$$

$$\to (KL)^2(2 - \beta)/(12\beta) \tag{32b}$$

for the long-rod limit, we have (cf. eq 9)

$$[\partial/\partial\tau - \bar{\Theta}(\nabla_\xi^2 - \bar{\mu}^2\xi^2)]g_K(\xi,\xi';\tau) = \delta(\xi - \xi')\delta(\tau) \tag{33}$$

Because β is very small (see later), $\bar{\mu} \gg 1$ does not necessarily mean $KL \gg 1$. The Green function will be given by simple replacement of μ and Θ in eq 23 or eq 27 with $\bar{\mu}$ and $\bar{\Theta}$, respectively. From eq 27, we have

$$g_K^{\mu}(\xi,\xi';\tau) = \operatorname{sech}(\bar{\mu}\bar{\Theta}\tau)\exp[-\bar{\mu}\xi^2\tanh(\bar{\mu}\bar{\Theta}\tau)]\delta(\xi - \xi') \qquad (\bar{\mu} \gg 1) \tag{34}$$

where use was made of an approximation[17]

$$\exp\left[-\frac{\bar{\mu}}{4}(\xi - \xi')^2/\tanh(\bar{\mu}\bar{\Theta}\tau)\right] = \left[\frac{4\pi}{\bar{\mu}}\tanh(\bar{\mu}\bar{\Theta}\tau)\right]^{1/2}\delta(\xi - \xi') \tag{35}$$

This approximation is valid only when $\bar{\mu} \gg 1$ and $KL \leq 3$, where $b_n(k)$ for $n \geq 2$ in eq 25 is negligibly smaller than $b_0(k)$. However, if we ignore the initial fast decay of $G^1(\tau)$ with a small amplitude due to the initial free rotation of the rod in the cage discussed in Appendix D, the above approximation will be valid for large KL values (see Appendix E). Then, we have $\bar{\mu} \gg 1$

$$G^1(\tau) = \exp(-\bar{D}_1K^2\tau)\operatorname{sech}(\bar{\mu}\bar{\Theta}\tau) \times \int_0^1 [j_0(k\xi)]^2\exp[-\bar{\mu}\xi^2\tanh(\bar{\mu}\bar{\Theta}\tau)]\,d\xi \tag{36}$$

To estimate the β-value, consider an imaginary cylinder (or a cage) enveloping the test rod with a radius a. If the mean number $N(a)$ of rods which touch this cylinder is known, we have $N(a_c) \simeq 1$. Doi[25] derived $N(a) = (1/2)\pi caL^2$, from which we have

$$\beta \simeq (cL^3)^{-2} \qquad \text{(Doi)} \tag{37a}$$

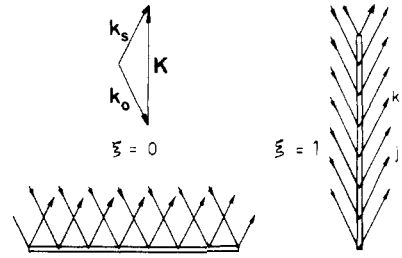

Figure 2. Scattering geometry showing the phase relationships between scattered rays from a rod at orientations $\xi = 0$ and ± 1 (for details, see text).

Because Doi and Edwards considered the case of $1 \ll cL^3 \ll L/d$, they assumed a very strong constraint, and actually they put $\bar{D}_1 = \bar{D}_2 = 0$. If we consider a case of $1 < cL^3 \ll L/d$, however, we have another approximation for estimating a_c and β. Because the volume of the cage can be approximated by a volume, $1/c$, occupied by one rod, we have $a_c \simeq (1/(cL))^{1/2}$. In this case, we have[26]

$$\beta \simeq (cL^3)^{-1} \qquad \text{(Mori et al.)} \tag{37b}$$

Since the latter β-value was derived under a rather weak constraint, the actual β-value will lie in between these two cases.

Since eq 33 is analogous to eq 9, eq 29 holds after simple replacement of D, D_i, and Θ with $\bar{D}$, $\bar{D}_i$, and $\bar{\Theta}$, respectively. The limiting forms are

$$\bar{\Gamma}/K^2 = D_3 + O(\beta D) \qquad (KL \leq 1 \text{ and } \bar{\mu} \gg 1) \tag{38a}$$

$$\to \beta[D_1 + (L^2/12)\Theta] = 2\beta D_1 \qquad (KL \gg 1) \tag{38b}$$

Except for the initial fast decay with a very small amplitude, $G^1(\tau)$ will decay with a very small decay rate as in eq 38b.

(3) Remarks. Since $g_K(\xi,\xi';0) = \delta(\xi - \xi')$ irrespective of the model, eq 20, 21, 23, and 34, the static intensity is given by

$$G^1(0) = \tfrac{1}{2}\int j_0(k\xi)^2\,d\xi = (1/L^2)\int\int j_0(K|s - s'|)\,ds\,ds' \tag{39}$$

For large k values, we have approximations $j_0(k\xi) = (\pi/k)\delta(\xi)$ and $j_0(K|s - s'|) = (\pi/K)\delta(s - s')$. Thus we have

$$G^1(0) \to \pi/(KL) \qquad (KL \gg 1) \tag{40}$$

At $\xi = 0$, all the scattered rays from a rod are in phase (Figure 2). At $\xi = \pm 1$, on the other hand, if rays j and k are out of phase, rays $j + i$ and $k + i$ are also out of phase for $i = 1, 2, \ldots$. The factor $j_0(k\xi)^2$ in eq 36 and 39 expresses this situation. For large k values, the scattered intensity from a solution of rods is exclusively contributed by those whose ξ-value is close to zero. This is a characteristic feature of the scattering from very long rods. This is the reason why D_3 does not contribute to $\bar{\Gamma}/K^2$ in eq 38b and also eq 30 (note that $D - \frac{1}{3}(D_3 - D_1) = D_1$, see eq 6).

The trajectory of the random motion of the rod in our model at semidilute regime is something like the contour of a Gaussian chain with a bond length L and a bond angle a_c/L. Once the rod axis is perpendicular to the vector $\vec{K}$, the rod stays at almost the same orientation for a long time and scatters the incident light strongly. After a very long time, the rod axis becomes parallel to the vector $\vec{K}$, and the rod scatters the incident light weakly (Figure 2).

Numerical Simulation and Discussion

We would like to present some computer simulation in order to visualize the theoretical results given above. [See Appendix F for algorithm of our computation.]

Table I
Numerical Values of $f_1(k)$ and $f_2(k)$

KL	$f_1(k)$	$f_2(k)$	KL	$f_1(k)$	$f_2(k)$
0.0	0.000000	0.333333			
1.0	0.011180	0.325933	21.0	0.845607	0.0300567
2.0	0.045480	0.303871	22.0	0.851958	0.0298148
3.0	0.104581	0.267989	23.0	0.857418	0.0294855
4.0	0.189024	0.221075	24.0	0.863091	0.0282469
5.0	0.294422	0.169448	25.0	0.869241	0.0262628
6.0	0.407904	0.123006	26.0	0.875256	0.0243804
7.0	0.510273	0.0911974	27.0	0.880356	0.0233128
8.0	0.586554	0.0765488	28.0	0.884331	0.0230467
9.0	0.635508	0.0729840	29.0	0.887688	0.0229480
10.0	0.667176	0.0715120	30.0	0.891123	0.0223787
11.0	0.692952	0.0666578	31.0	0.894942	0.0212334
12.0	0.718713	0.0583525	32.0	0.898854	0.0199547
13.0	0.744150	0.0498826	33.0	0.902331	0.0190863
14.0	0.766101	0.0444110	34.0	0.905103	0.0187905
15.0	0.782613	0.0424927	35.0	0.907392	0.0187490
16.0	0.794691	0.0421649	36.0	0.909663	0.0184891
17.0	0.805053	0.0410198	37.0	0.912213	0.0178059
18.0	0.815760	0.0381314	38.0	0.914934	0.0169076
19.0	0.826929	0.0343974	39.0	0.917469	0.0161909
20.0	0.837273	0.0314212	40.0	0.919545	0.0158766
			∞	1.000000	0.0000000

(1) Rigid Rod in Dilute Solution. Since the initial decay rate $\bar{\Gamma}$ of $G^1(\tau)$ for a dilute solution of rigid rods is given by eq 29 with functions $f_1(k)$ and $f_2(k)$ defined by eq B5 and B6 in Appendix B, their numerical values are given in Table I. Wilcoxon and Schurr[16] have given the corresponding functions $G(k)$ and $F(k)$ on the basis of a different model from ours. Their $G(k)$ equals our $f_1(k)/24$ and their $F(k)$ equals our $(1 - f_2(k))/2$. Their computed values are different from ours by 1% or less in $F(k)$ and by 2–4% in $G(k)$. However, this difference was found to come from the degree of accuracy of their numerical computation; our computation of their $G(k)$ and $F(k)$ showed that both relations, $G(k) = f_1(k)/24$ and $F(k) = (1 - f_2(k))/2$, hold for up to six digits, i.e., within the precision of our computation. Figure 3 shows the above result graphically. When experimental $\bar{\Gamma}/K^2$ exceeds the theoretical one, we have to consider a possible contribution from internal bending motions of rods as given below.

(2) On the Size of Matrix M. There arises a question: How large a size of the matrix **M** in eq 15 is required in order to obtain reasonable result? Since the matrix elements $a_{n,n}$ and $a_{n,n\pm2}$ tend toward $n^2 + \mu^2/2$ and $\mu^2/4$, respectively, for large n's, there may be no problem if we truncate A_n in eq 12 at $n = N$ for which $N(N+1) \simeq 100\mu^2$ holds. For this choice of N, numerical results actually showed that the difference between the largest eigenvalue λ_N and $N(N+1)$ was less than 0.5%. For $\mu = 10$, for example, we have $N \simeq 100$ or matrix size $\simeq 50 \times 50$. In computing $G^1(\tau)$, on the other hand, we can terminate the summation over n in eq 24 at $n = N'$ for which $(2N'+1)b_{N'}(k)^2 \leq 10^{-6}G^1(0)$. During simulation of $G^1(\tau)$'s, we empirically found that this N' value was about twice larger than that from our criterion,[27] $K^2\langle\delta_n^2\rangle = [2/n(n+1)]\mu^2 \geq 1$ in eq D3 in Appendix D. For $\mu = 10$, we have $N' = 28$. There is a big difference between N and N'. However, we have to consider the fact that the coupling occurs only between A_n and $A_{n\pm2}$ in eq 12. So, the eigenvalues λ_p for $p \leq N'$ are expected to converge to their final value much faster than λ_N does to $N(N+1)$ with an increasing N value. A numerical study suggested that the matrix size of $((N/2)+1, (N/2)+1)$ with $N = 2N'$ was large enough to have accurate results of $G^1(\tau)$, i.e., within a relative error of 10^{-6}. Halving the matrix size still gave $G^1(\tau)$ with a relative error less than 1%.

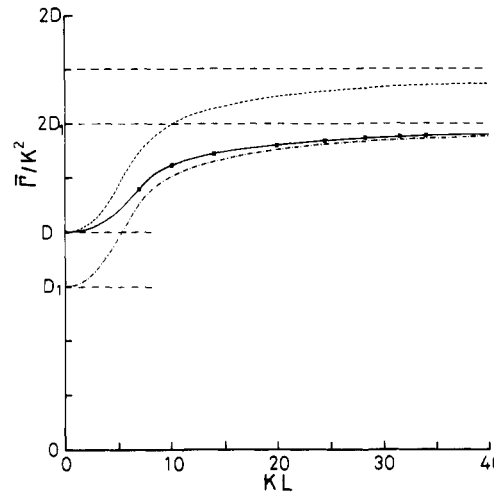

Figure 3. $\bar{\Gamma}/K^2$ vs. KL relation for a dilute solution of monodisperse rigid rods. The long-rod limit, $D_3 = 2D_1$ and $\Theta = 12D_1/L^2$, was assumed: (—) from eq 29; (···) from eq 29 with $f_2(k) = {}^1/_3$ (isotropic); (–·–) from eq 29 with $f_2(k) = 0$ (see later) and (– – –) asymptotes; (■) from the cumulant analysis of simulated correlation functions shown in Figure 4.

(3) Accuracy of the Harmonic Oscillator Model. To test the accuracy of the correlation functions $G^1(\tau)$ based on eq 28, which used the Green function derived from the harmonic oscillator model, we computed $G^1(\tau)$ based on eq 24 and 28. Results are shown in Figure 4, which indicates that when $\mu^2 \equiv (KL)^2/12 = 50$, $G^1(\tau)$ based on eq 28 is different *at most* by 2% from $G^1(\tau)$ based on eq 24 within the entire range of delay times of interest. As far as the simulation of correlation functions is concerned, the harmonic oscillator model works very well *for μ values as small as* 7. (This does not necessarily mean that the Green function $g_K^{\gg}(\xi,\xi';\tau)$ in eq 23 itself is a good approximation for μ values down to 7. The first two eigenvalues λ_0 and λ_2, of the matrix **M** and $(2n+1)\mu$ for $n = 0$ and 2 of the harmonic oscillator model (see eq 22), are compared in Table II, from which we can infer that for $\mu^{1/2} \geq 10$, both Green functions in eq 20 and 23 agree well.)

The computed correlation functions were analyzed by use of a third-order cumulant expansion method, and the results are shown in Figure 3.

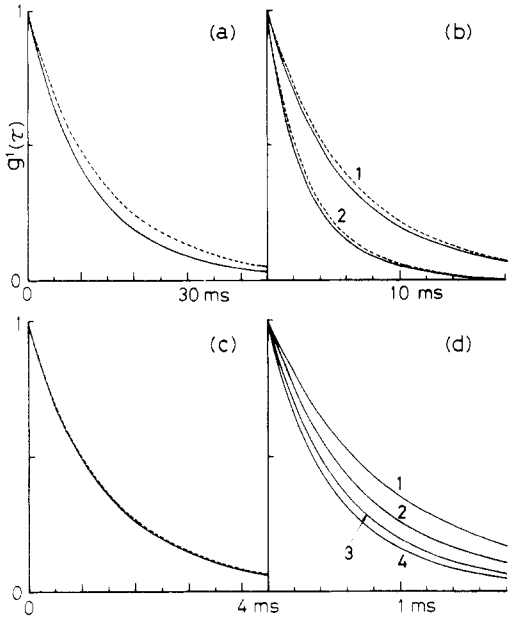

Figure 4. Examples of simulated correlation functions for a dilute solution of monodisperse rigid rods. Parameter values are L = 1 μm, $D = 1.32 \times 10^{-8}$ cm^2/s ($D_3 = 2D_1$ and $\Theta = 12D_1/L^2$): (---) from eq 24 (truncation method); (—) from eq 28 (harmonic oscillator model). (a) At $K^2 = 0.5 \times 10^{10}$ cm^{-2} ($\mu^2 = 4.2$ and **M** size = 7 × 7). (b) 1, at $K^2 = 1.0 \times 10^{10}$ cm^{-2} ($\mu^2 = 8.3$ and 7 × 7); 2, at $K^2 = 2.0 \times 10^{10}$ cm^{-2} ($\mu^2 = 16.7$ and 7 × 7). (c) At $K^2 = 4.0 \times 10^{10}$ cm^{-2} ($\mu^2 = 33.3$ and 11 × 11). (d) 1, at $K^2 = 6.0 \times 10^{10}$ cm^{-2} ($\mu^2 = 50.0$ and 11 × 11); 2, at $K^2 = 8.0 \times 10^{10}$ cm^{-2} ($\mu^2 = 66.7$ and 11 × 11); 3, at $K^2 = 10.0 \times 10^{10}$ cm^{-2} ($\mu^2 = 83.3$ and 21 × 21); 4, at $K^2 = 11.7 \times 10^{10}$ cm^{-2} ($\mu^2 = 97.5$ and 21 × 21). In part d, both --- and — superimpose with each other within the thickness of lines at each K^2 value.

Table II
Comparison of the First Two Eigenvalues λ_0 and λ_2 of the Matrix M and $(2n + 1)\mu$ for n = 0 and 2 of the Harmonic-Oscillator Model

μ^2	10^2	10^3	10^4	10^5	10^6
λ_0/μ	0.923	0.976	0.992	0.998	0.999
$\lambda_2/5\mu$	0.917	0.976	0.992	0.998	0.999
size[a]	—/11	11/21	11/21	31/41	71/81
$\mu^{1/2}$	3.16	5.62	10.0	17.8	31.6

[a] 11/21, for example, means that the final values for λ_0 and λ_2 were obtained at a matrix size between 11 × 11 and 21 × 21.

(4) Rigid Rod in Semidilute Solution. At this regime, $\bar{\mu}^2 \simeq (KL)^2/6\beta$, so that, except for very small KL's, $\bar{\mu}$ is very large provided that β is small. For an accessible range of K values, we can use the Green function derived from the harmonic oscillator model. Here, we would like to show how the approximation in eq 35 works. For this purpose, we computed $G^1(\tau)$'s based on eq 36 and 28 (with replacement of μ, D_1, and Θ by $\bar{\mu}$, $\bar{D}_1$, and $\bar{\Theta}$, respectively). We also used eq 24 (with replacement of μ, D_1, and Θ by $\bar{\mu}$, $\bar{D}_1$, and $\bar{\Theta}$, respectively). Figure 5 depicts some examples of the simulated correlation functions for $\beta \equiv 1/(cL^3)^2 = 1/1600$ (see eq 37a). In this case, we could not observe appreciable difference between $G^1(\tau)$'s based on eq 24, 28, and 36. It should be noted that the decay of correlation functions at this regime is very slow.

Figure 6 depicts examples of the simulated correlation functions for $\beta \equiv 1/(cL^3) = 1/40$ (see eq 37b). In this case, both eq 24 and 28 gave the same decay curves, but eq 36 gave different decay curves from the above ones at larger KL's. The approximation in eq 35 is no longer valid at this β value.

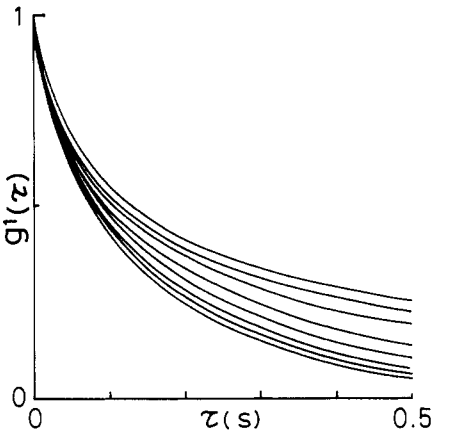

Figure 5. Examples of simulated correlation functions for a semidilute solution of monodisperse rigid rods. Parameter values are the same as those in Figure 4 except for $\beta = 1/1600$. $10^{-10}K^2$ values are, from top to bottom, 0.5, 1.0, 2.0, 4.0, 6.0, 8.0, 10.0, and 11.7 cm^{-2}. $G^1(\tau)$'s based on eq 24, 28, and 36 coincide with each other within 0.1% relative errors over the entire range of the delay time of interest.

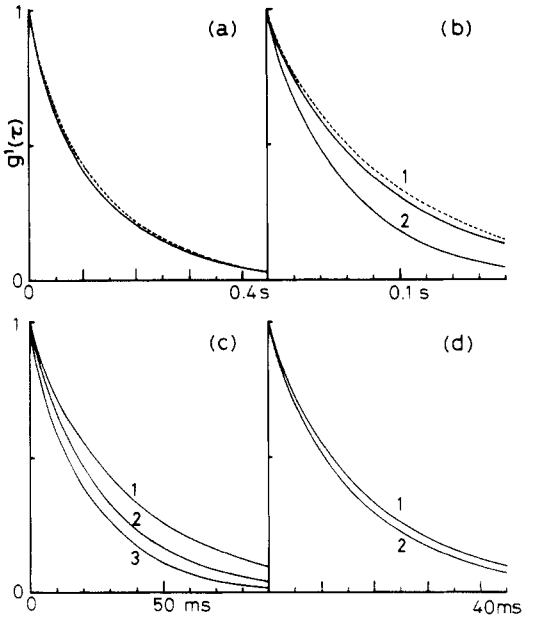

Figure 6. Examples of simulated correlation functions for a semidilute solution of monodisperse rigid rods. Parameter values are the same as those in Figure 5 except for $\beta = {}^1/_{40}$: (---) based on eq 36; (—) based on eq 24 and 28.

(5) Further Approximation. Equation 24 is rewritten as

$$G^1(\tau) = G_D(\tau)\sum_n\sum_l [\mathbf{W}(\tau)]_{nl} b_n(k) b_l(k) \qquad (41)$$

where

$$\mathbf{W}(\tau) = \{b_{nl}(\tau)\} \qquad (42)$$

with

$$b_{nl}(\tau) = (2l + 1)(i)^n(-i)^l[\mathbf{U} \exp(-\Lambda\Theta\tau)\mathbf{U}^{-1}]_{nl} \qquad (43)$$

$$= (2l + 1)(i)^n(-i)^l\sum_p U_p(n)U_p^*(l) \exp(-\lambda_p\Theta\tau) \qquad (44)$$

The matrix $\mathbf{W}(0)$ is diagonal with elements $b_{nn}(0) = (2n + 1)$ because $\mathbf{U}\mathbf{U}^{-1} = \mathbf{E}$ or $\sum_p U_p(n)U_p^*(l) = \delta_{nl}$. As τ becomes larger, the off-diagonal elements of $\mathbf{W}(\tau)$ appear. But, because of the time behavior of the matrix $\mathbf{U}\exp(-\Lambda\Theta\tau)\mathbf{U}^{-1}$, $b_{nl}(\tau)$ with larger n and/or l rapidly disappear

Table III
Time Evolution of the Matrix $\mathbf{W}(\tau)$[a,b]

0	2	4	6	8	10	1	14	16	18	20	22	24
579	45	0	0									
	2792	111	1	0								
		4870	170	2	0							
1391			6680	219	3	0						
500	5857			8135	257	3	0					
46	1088	8975			9183	282	4	0				
2	84	1407	10000			9800	294	4	0			
0	4	102	1419	9163			10000	294	4	0		
	0	4	95	1027	7210			9820	284	3	0	
		0	4	76	892	4971			9325	266	3	0
			0	3	53	581	3037			8548	241	3
				0	2	33	337	1655			7680	213
					0	1	18	174	808			6689
						0	0	9	81	354		
							0	0	4	34	140	
								0	0	1	12	49

[a] Two cases (τ = 0.2 and 1 ms) are shown for $K^2 = 6.0 \times 10^{10}$ cm^{-2}, L = 1.0 μm, and $D = 1.32 \times 10^{-8}$ cm^{-2}/s ($D_3 = 2D_1$ and $\theta = 12D_1/L^2$). Since matrices are symmetrical, only half of the elements are shown for each case. To make clear the relative sizes of the elements, the value of the largest element is normalized to 10000. [b] Upper right, τ = 0.2 ms and max = 16.61; lower left, τ = 1 ms and max = 5.895.

with a further increase of τ. This will be easily seen from the first-order perturbation results (see Appendix G):

$$b_{nn}(\tau) = (2n + 1)e^{-\lambda_n\theta\tau} \tag{45a}$$

$$b_{n,n-2}(\tau) = -(2n - 3)\mu^2L_1(n)[e^{-\lambda_n\theta\tau} - e^{-\lambda_{n-2}\theta\tau}]/(\lambda_n - \lambda_{n-2}) \tag{45b}$$

$$b_{n,n+2}(\tau) = -(2n + 5)\mu^2L_2(n)[e^{-\lambda_n\theta\tau} - e^{-\lambda_{n+2}\theta\tau}]/(\lambda_n - \lambda_{n+2}) \tag{45c}$$

$$b_{nl}(\tau) = 0 \qquad (l \neq n, n \pm 2) \tag{45d}$$

where $\lambda_n = n(n + 1) + \mu^2L_0(n)$. Note that both $b_{n,n-2}(\tau)$ and $b_{n,n+2}(\tau)$ are *nonnegative* because of $\lambda_{n+2} > \lambda_n$. Since $L_1(0) = 0$ and $(2n + 1)L_1(n + 2) = (2n + 5)L_2(n)$, we have a relation $b_{n+2,n}(\tau) = b_{n,n+2}(\tau)$, that is, the matrix $\mathbf{W}(\tau)$ is symmetrical. (Equation 45 is valid only for small μ^2). Table III shows examples of the time evolution of the matrix $\mathbf{W}(\tau)$ in eq 42–44. From these examples, we can infer that the summation over l in eq 41 can be limited only to $l = n$ (diagonal) and $l = n \pm 2$ (the first off diagonal). To see this, we computed eq 41 with all elements $b_{nl}(\tau)$, the diagonal and the first off-diagonal elements $b_{nn}(\tau)$ and $b_{n,n\pm2}(\tau)$, and the diagonal and the first and the second off-diagonal elements $b_{nn}(\tau)$, $b_{n,n\pm2}(\tau)$, and $b_{n,n\pm4}(\tau)$. The results indicated that for $\mu^2 \leq 50$, eq 41 with only the diagonal and the first off-diagonal elements gives accurate results enough to simulate $G^1(\tau)$ for rods.

(6) Note on Further Application. In another paper,[28] the experimental results on thick myofilament suspensions[12] were analyzed by use of our old model on $G^1(\tau)$ for semiflexible filaments.[20] So, we would like to add a few remarks on that model.

Equation 29 can be written as

$$\bar{\Gamma}/K^2 = [D - \tfrac{1}{3}(D_3 - D_1)(1 - 3f_2(k))] + (L^2/12)\theta f_1(k) \tag{46}$$

The anisotropic translation of a rod appears as a factor $(1 - 3f_2(k))$ in eq 46. The dash–dot line in Figure 3 represents eq 46 with $f_2(k) = 0$ irrespective of the k values. At $KL \geq 30$, there is no appreciable difference between the solid line and the dash–dot one in Figure 3. This means that the original Pecora formula, eq 26, with replacement of D by D_1 or $[D - {}^1/_3(D_3 - D_1)]$ will work very well for $KL \geq 30$.

In our previous paper, we have considered the effect of the filament flexibility in a way that (see Appendix D in ref 20)

$$J(s,s',\tau) = e^{-DK^2\tau}\langle e^{iK(s\xi - s'\xi')}\rangle_{\text{rot}} \prod_{m\geq 2} e^{-\Phi(m,s,s',\tau)} \tag{47}$$

$$\Phi(m,s,s',\tau) = (K^2/6)\langle q_m{}^2\rangle[Q(m,s)^2 + Q(m,s')^2 - 2Q(m,s)Q(m,s')e^{-\tau/\tau_m}] \tag{48}$$

Using eq 21 for computation of the expectation value $\langle\cdots\rangle_{\text{rot}}$ in eq 47, we have

$$G^1(\tau) = (1/L^2)\int\int_{-L/2}^{L/2}\sum_n(2n + 1) \times e^{-[DK^2+n(n+1)\theta]\tau}j_n(Ks)j_n(Ks')\prod{}''e^{-\Phi(m,s,s',\tau)}\,ds\,ds' \tag{49}$$

where the summation has to be carried out over even and odd n, because $\prod''\exp[-\Phi(m,s,s',\tau)]$ is neither an even nor odd function of both s and s'. From eq 49 we have[20]

$$\bar{\Gamma}/K^2 \to D + (L^2/12)\theta + D_1\Sigma''1 \qquad (KL \gg 1) \tag{50}$$

where $\Sigma''1$ means the number of internal modes of bending motion involved in the scattering process. By comparison of eq 50 with eq 46, a simple replacement of D in our old model[20] with D_1 or $[D - {}^1/_3(D_3 - D_1)]$ would work correctly for the case of a semiflexible filament at $KL \geq 30$. When we use eq 20, we have from eq 47

$$G^1(\tau) = G_D(\tau) \times (1/L^2)\int\int_{-L/2}^{L/2}\sum_n\sum_l b_{nl}(\tau)j_n(Ks)j_l(Ks')\prod{}''e^{-\Phi(m,s,s',\tau)}\,ds\,ds' \tag{51}$$

which gives

$$\bar{\Gamma}/K^2 \to [D - \tfrac{1}{3}(D_3 - D_1)] + (L^2/12)\theta + D_1\Sigma''1 \qquad (KL \gg 1) \tag{52}$$

In eq 51, $b_{nl}(\tau)$ for even n and l is given by eq 44. For odd n and l, we have to solve another eigenvalue problem similar to eq 17. Details will be discussed elsewhere, where we will also consider the effect of ξ and ξ' on the internal factor $\Phi(m,s,s',\tau)$.

Conclusions

We have considered the effect of anisotropic diffusion on the polarized-field correlation function $G^1(\tau)$ of light quasielastically scattered from solutions of very long rods. Without solving a coupled translational/rotational diffusion equation, we obtained an expression for the first cumulant of $G^1(\tau)$ as given in eq 29, which is exactly the same as the previous result from another approach.[16] By applying the truncation method[14] and the harmonic-oscillator model,[17] we obtained the Green function to the coupled diffusion equation as given in eq 20 and 23. Using this Green function, we formulated the expression of $G^1(\tau)$ for dilute solutions of rods as given in eq 24 and 28. These results are applicable to the case of semidilute solutions after simple replacement of μ, D, D_i, and Θ with $\bar{\mu}$, $\bar{D}$, $\bar{D}_i$, and $\bar{\Theta}$, respectively. Our method requires machine computation, because it is oriented to treat the case of very long rods. For shorter rod lengths, we can formulate $G^1(\tau)$ in an analytical form. As shown in Appendix G, our result includes the previous ones for shorter rod lengths.[13-15] Some examples of simulated $G^1(\tau)$'s for rods were presented in order to estimate the accuracy of approximations and to visualize the theory. At dilute regime, the harmonic-oscillator model works well for μ^2 values as small as 50 as shown in Figure 4. At semidilute regime, for β $[\equiv(a_c/L)^2] \ll 1$ and hence $\bar{\Theta} \ll \Theta$ (where $\bar{\mu}^2 \gg 1$ except for extremely small KL values), the Doi–Edwards approximation, eq 35, is valid and eq 36 works for larger KL values as shown in Appendix E and in Figure 5. On the other hand, when $\bar{\mu}^2$ is very large but β and hence $\bar{\Theta}$ are not very small, the harmonic-oscillator model can work correctly but eq 35 fails to hold as shown in Figure 6. For a very long rod with a finite thickness, violation of the Rayleigh–Debye condition will occur, so that our result is qualitative at small K values. But, for large KL *and* large K values, our result will be quantitatively correct as mentioned in the Model section.

The perturbation result, e.g., eq G8 in Appendix G, will work, at most, for $\mu^2 \leq 7$ (TMV in dilute solution for λ = 488 nm), where the $n = 0$ and 2 modes are predominant. In such a case, in addition to the first-cumulant analysis with eq 29, a two-exponential analysis will be possible and an analytical expression of $G^1(\tau)$ may be useful. When $\mu^2 > 7$, on the other hand, it may be more practical to compare the profiles of experimental $G^1(\tau)$ with those of computed ones at various combinations of D_i and Θ. Our method permits computation of $G^1(\tau)$ by use of a "desktop" computer.

In a study under progress, we are testing with success the present theory (at dilute regime) not only on the first cumulant of, but also on the profiles themselves of $G^1(\tau)$. For a case of a very long rod where the present method will show its full power, we have to inevitably take account of the filament flexibility.[18b] The Green function obtained here can be used to formulate an expression of $G^1(\tau)$ for solutions of semiflexible filaments at dilute and semidilute regimes. These will be discussed in another paper in the near future.[35]

Appendix A. Some of the Algebraic Manipulation

(1) Derivation of Eq 12. Using $(n+1)P_{n+1}(\xi) - (2n+1)\xi P_n(\xi) + nP_{n-1}(\xi) = 0$, we have

$$\xi^2 P_n(\xi) = \frac{1}{2n+1}\left[\frac{(n+1)(n+2)}{2n+3}P_{n+2}(\xi) + \frac{(2n+1)(2n^2+2n-1)}{(2n-1)(2n+3)}P_n(\xi) + \frac{n(n-1)}{2n-1}P_{n-2}(\xi)\right] \quad \text{(A1)}$$

Using the orthonormality condition for $P_n(\xi)$, we have from eq A1

$$\sum_m A_m \int_{-1}^{1} \xi^2 P_m(\xi) P_n(\xi)\, d\xi = \frac{2}{2n+1}[L_0(n)A_n + L_1(n)A_{n-2} + L_2(n)A_{n+2}] \quad \text{(A2)}$$

where $L_i(n)$ (i = 0, 1, and 2) are given by eq 13. Since $g_K(\xi,\xi';0) = \delta(\xi - \xi')$, eq 10 gives eq 11. Substituting eq 10 into eq 9, multiplying both sides by $P_m(\xi)$, and integrating over ξ, we obtain eq 12 for $\tau > 0$, where formula A2 and a relationship $\nabla_\xi^2 P_n(\xi) = -n(n+1)P_n(\xi)$ were used. The formula

$$\int_{-1}^{1} \exp(\pm iz\xi) P_n(\xi)\, d\xi = 2(\pm i)^n j_n(z) \quad \text{(A3)}$$

will be used to obtain eq 24 and others, where $j_n(z)$ is the nth order spherical Bessel function.

(2) Derivation of Eq 28. In terms of the new variables

$$\eta = \frac{\xi + \xi'}{2} \qquad \eta' = \frac{1}{\kappa}\frac{\xi - \xi'}{2} \quad \text{(A4)}$$

with $\kappa^2 = \tanh(\mu\Theta\tau)/\mu$ eq 27 is written as

$$g_K^{\gg}(\xi,\xi';\tau)\, d\xi\, d\xi' = (1/\pi^{1/2}) \operatorname{sech}(\mu\Theta\tau) e^{-(\mu\kappa\eta)^2} e^{-\eta'^2}\, d\eta\, d\eta' \quad \text{(A5)}$$

By using eq A4 and A5, eq 8 for $\mu \gg 1$ is written as

$$J_\theta(s,s',\tau) = (1/2\pi^{1/2}) \operatorname{sech}(\mu\Theta\tau) \int_{-1}^{1} I(\eta) e^{iK(s-s')\eta} e^{-(\mu\kappa\eta)^2}\, d\eta \quad \text{(A6)}$$

where

$$I(\eta) = \int_{-\rho}^{\rho} e^{iK(s+s')\kappa\eta'} e^{-\eta'^2}\, d\eta' \qquad (\rho = (1 - |\eta|)/\kappa) \quad \text{(A7)}$$

Since $\kappa \ll 1$ (or $\mu \gg 1$), $I(\eta)$ is very close to the limiting value of $I(0)$ except for η values very close or equal to ± 1. Thus, we can approximate $I(\eta)$ by extending ρ to infinity. Then, we have an approximate form

$$J_\Theta(s,s',\tau) = \operatorname{sech}(\mu\Theta\tau) e^{-[K(s+s')\kappa/2]^2} \frac{1}{2}\int_{-1}^{1} e^{iK(s-s')\eta} e^{-(\mu\kappa\eta)^2}\, d\eta \qquad (\kappa \ll 1 \text{ or } \mu \gg 1) \quad \text{(A8)}$$

In terms of the new variables $u = s + s'$ and $v = s - s'$, integration of eq A8 over v can be carried out. After transformation by $y = K(L - u)$, eq 1, 7, and A8 give eq 28.

Appendix B. Initial Decay Rate $\bar{\Gamma}$ of $G^1(\tau)$ for Rods

Equations 8, 10, and A3 in Appendix A give

$$J_\Theta(s,s',\tau) = \sum_n (i)^n j_n(Ks) \int_{-1}^{1} e^{-iKs'\xi'} A_n(K,\xi',\tau)\, d\xi' \quad \text{(B1)}$$

Equations 11 and 12 give

$$-2\partial A_n(K,\xi',\tau)/\partial\tau|_{\tau=0} = n(n+1)(2n+1)\Theta P_n(\xi') + (D_3 - D_1)K^2[(2n+1)L_0(n)P_n(\xi') + (2n-3)L_1(n)P_{n-2}(\xi') + (2n-5)L_2(n)P_{n+2}(\xi')] \quad \text{(B2)}$$

Integration of a recurrence formula $dj_n(z)/dz = [nj_{n-1}(z) - (n+1)j_{n+1}(z)]/(2n+1)$ gives after changing n

$$b_{n+2}(k) = \frac{n+1}{n+2} b_n(k) - \frac{2n+3}{n+2} j_{n+1}(k)/k \quad \text{(B3)}$$

where $b_n(k)$ is given by eq 25. Using these results, we have from $\bar{\Gamma} = -(\partial/\partial\tau) \ln G^1(\tau)$ at $\tau = 0$

$$\bar{\Gamma}/K^2 = [D - \tfrac{1}{3}(D_3 - D_1)] + (L^2/12)\Theta f_1(k) + (D_3 - D_1)f_2(k) \quad \text{(B4)}$$

where

$$f_1(k) = (3/k^2)[\sum_n n(n+1)(2n+1)b_n(k)^2]/G^1(0) \quad \text{(B5)}$$

$$f_2(k) = [\sum_{\text{even } n} (2n+3)\{j_{n+1}(k)/k\}^2]/G^1(0) \quad \text{(B6)}$$

where $G^1(0) = \sum_n (2n+1)b_n(k)^2$. The contribution from terms in [···] in eq B2 can be written in a concise form as in eq B6 by multiple use of eq B3. For small k, we have $j_{n+1}(k)/k = k^n/(2n+3)!!$ and $b_0(k) = 1 - k^2/18$. Thus, we have the limiting values of $f_1(0) = 0$ and $f_2(0) = {}^1/_3$ as they should be.

If we regard eq 12 to be the recurrence formula for $\partial A_n/\partial\tau$ at $\tau \to 0$, we have $\partial^2 A_n/\partial\tau^2$ at $\tau = 0$ immediately. Thus, we can compute the second cumulant μ_2 in the same way as above.

It is evident that $\lim\ (\partial/\partial\tau)[\mathbf{U}\ \exp(-\mathbf{\Lambda}\Theta\tau)\mathbf{U}^{-1}] = -\Theta\mathbf{U}\mathbf{\Lambda}\mathbf{U}^{-1} = -\Theta\mathbf{M}$ and $\lim\ (\partial^2/\partial\tau^2)[\mathbf{U}\ \exp(-\mathbf{\Lambda}\Theta\tau)\mathbf{U}^{-1}] = \Theta^2\mathbf{M}^2$, where "lim" means to take the limiting value at $\tau = 0$ of its operand. Without detailed information on $\mathbf{\Lambda}$ and $\mathbf{U}$, therefore, eq 24 gives the same results as above from the same procedure.

Appendix C. $\bar{\Gamma}$ for Rods at $KL \gg 1$

Since we need the initial form of $G^1(\tau)$, hyperbolic functions in eq A8 are expanded up to the first power of $(\mu\Theta\tau)$:

$$J_\Theta(s,s',\tau) = \exp[-K^2(s+s')^2\Theta\tau/4]\frac{1}{2}\int_{-1}^{1} e^{iK(s-s')\eta}e^{-\mu^2\Theta\tau\eta^2}\,d\eta \quad \text{(C1)}$$

from which we have

$$-\partial J_\Theta(s,s',\tau)/\partial\tau|_{\tau=0} = [\Theta K^2(s+s')^2/4]j_0(K|s-s'|) + (D_3 - D_1)K^2\frac{1}{2}\int_{-1}^{1}\eta^2 e^{iK(s-s')\eta}\,d\eta \quad \text{(C2)}$$

Integration of eq C2 over s and s' gives eq B4 with

$$f_1(k) = (3/L^2)(1/L^2)\int\int_{-L/2}^{L/2}(s+s')^2 j_0(K|s-s'|)\,ds\,ds'/G^1(0) \quad \text{(C3)}$$

$$f_2(k) = (1/2)\int_{-1}^{1}\eta^2 j_0(k\eta)^2\,d\eta/G^1(0) \quad \text{(C4)}$$

where $G^1(0)$ is given by eq 39. Since $j_0(kz) \to (\pi/k)\delta(z)$ as $k \to \infty$, we have the limiting values of $f_1(\infty) = 1$ and $f_2(\infty) = 0$; that is

$$\bar{\Gamma}/K^2 \to [D - \tfrac{1}{3}(D_3 - D_1)] + (L^2/12)\Theta \qquad (KL \gg 1) \quad \text{(C5)}$$

Similarly, the second cumulant μ_2 can be computed. From eq C1, we have $\mu_2 = (4/5)(\Theta K^2L^2/12)^2$. The normalized dispersion $\mu_2/\bar{\Gamma}^2$ of $G^1(\tau)$ is thus equal to ${}^1/_5$ when $k \gg 1$, because in the long-rod limit, $D_3 = 2D_1$ and $\Theta = 12D_1/L^2$ and hence $\bar{\Gamma} = 2D_1K^2$.

Appendix D. Rotational Brownian Motion in a Cage

From the first exponential factor in eq 27, we have

$$\langle(\xi - \xi')^2\rangle = (2/\mu)\tanh(\mu\Theta\tau) \quad \text{(D1)}$$

For short times, eq D1 becomes $\langle(\xi - \xi')^2\rangle = 2\Theta\tau$, which is just the Einstein relation for the rotational Brownian motion without restriction. Let us consider eq 26 for simplicity of discussion. The expectation value of $(\xi - \xi')^2$ for the nth component of the rotational motion is given by

$$\langle(\xi - \xi')^2\rangle_n = 2\Theta\tau_n^r = 2/[n(n+1)] \quad \text{(D2)}$$

because the rotational relaxation time is given by $\tau_n^r = 1/[n(n+1)\Theta]$. Then, the product of K^2 and the "mean amplitude" of the lateral fluctuation of the rod $\langle\delta_n^2\rangle$ is given by[27]

$$K^2\langle\delta_n^2\rangle = \frac{2}{n(n+1)}\frac{(KL)^2}{12} \quad \text{(D3)}$$

when $K^2\langle\delta_n^2\rangle \gtrsim 1$, the nth component will contribute to $G^1(\tau)$. From eq D3, we have, for example, $n \lesssim 12$ for $KL = 30$. Now, consider a cage (whose radius is a_c and lifetime is $\tau_{cage} = L^2/2D_3$ ($\equiv L^2/4D_1$); see text) which confines a rod. The rod will freely rotate up to time τ_0:

$$(a_c/L)^2 = 2\Theta\tau_0 \quad \text{(D4a)}$$

or

$$\tau_0 = (a_c/L)^2/(2\Theta) \equiv a_c^2/(24D_1) \quad \text{(D4b)}$$

Then, the ratio of τ_0/τ_{cage} will be $\simeq (a_c/L)^2/6$ (see Figure 7). From these considerations, we have for $KL = 30$, for example

$$P_\Theta(\tau_0) = \sum_{n=0}^{12}(2n+1)b_n(k)^2 e^{-n(n+1)(a_c/L)^2/2} \quad \text{(D5)}$$

As mentioned in the Introduction, 1 mg/mL of thin filament concentration corresponds to $cL^3 = 40$. Since $(a_c/L) \simeq (cL^3)^{-1}$ (see text), $P_\Theta(\tau)$ will decay only a few percent of its initial value within the lifetime of the cage. This means that except for very short times, the rotational motion will not contribute to $G^1(\tau)$ even at large KL values *in the case of semidilute solutions*. Figure 7b depicts this situation.

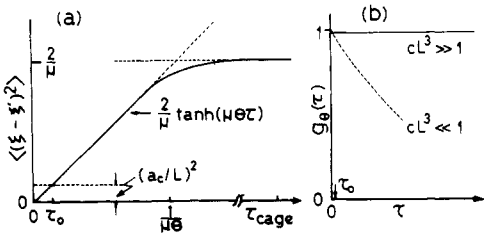

Figure 7. (a) A graphic representation of the $\langle(\xi - \xi')^2\rangle$ vs. τ relation. (See text for τ_0, $1/(\mu\Theta)$, and τ_{cage} on the time axis, and $2/\mu$ and $(a_c/L)^2$ on the vertical axis.) (b) A schematic representation of the time behavior of $g_\Theta(\tau)$. $g_\Theta(\tau) = P_\Theta(\tau)/P_\Theta(0)$ and $P_\Theta(\tau)$ is given by eq D5.

Appendix E. On the Validity of Eq 35

Equations 8 and 34 give

$$J_\Theta(s,s',\tau) = \frac{1}{2}\int_{-1}^{1} e^{iK(s-s')\xi}e^{-\bar{\mu}^2\bar{\Theta}\tau\xi^2}\,d\xi \qquad (\bar{\mu}\bar{\Theta}\tau \le 0.1) \quad \text{(E1)}$$

Without the assumption in eq 35, on the other hand, we have from eq C1 (after changing μ and Θ with $\bar{\mu}$ and $\bar{\Theta}$, respectively)

$$J_\Theta(s,s',\tau) = e^{-\bar{\Theta}K^2(s+s')^2\tau/4}\frac{1}{2}\int_{-1}^{1} e^{iK(s-s')\eta}e^{-\bar{\mu}^2\bar{\Theta}\tau\eta^2}\,d\eta \qquad (\bar{\mu}\bar{\Theta}\tau \le 0.1) \quad \text{(E2)}$$

Now, we have relationships

$$\bar{\mu}\bar{\Theta}\tau = D_3K^2\tau\frac{6^{1/2}}{KL}(a_c/L) \quad \text{(E3)}$$

$$\bar{\Theta}K^2\tau(s + s')^2 = \bar{\mu}\bar{\Theta}\tau\frac{3}{2(6^{1/2})}KL(a_c/L)\left(\frac{s + s'}{L/2}\right)^2 \quad \text{(E4)}$$

For $\bar{\mu}\bar{\Theta}\tau = 0.1$, $KL = 30$ and $a_c/L = {}^1/_{40}$, eq E4 gives $\bar{\Theta}K^2(s + s')^2/4 \leq {}^1/_{20}$. This means that the first exponential in eq E2 is practically unity when s and s' are varied; that is, eq E1 and E2 are the same with each other for the assumed conditions. From eq E3, the condition $\bar{\mu}\bar{\Theta}\tau = 0.1$ implies $D_3K^2\tau = (1/10)(KL/6^{1/2})(L/a_c) = 4$ for $KL = 2.5$ and 40 for $KL = 25$. Thus, for such long times as $D_3K^2\tau \leq 4$ (or 40 at larger KL's), the approximation in eq 35 is quite valid. This comes solely from the smallness of the (a_c/L) value.

In the previous paper,[21] we carelessly assumed an approximation like eq 35 for $\mu \gg 1$ (and not $\bar{\mu} \gg 1$), so that we could not obtain non-zero $f_1(k)$ in eq C3.

Appendix F. Algorithm of Numerical Computation

(1) Computation of Eigenvalues and Eigenvectors of M. Since the matrix **M** given in eq 15 is a real tridiagonal matrix whose off-diagonal elements are all nonnegative, **M** can be transformed to a real symmetric tridiagonal matrix by using a similarity transformation. The symmetrized matrix and the transformation matrix are used to find the eigenvalues and the eigenvectors of the matrix **M**.[29]

(2) Numerical Computation of $G^1(\tau)$ at $\mu \gg 1$. The double integration in eq 28 was carried out with an adaptive N-dimensional quadrature subroutine.[30] We usually compute $G^1(\tau)$ with 0.1% error tolerance.

Appendix G. Relationships with Previous Theories

Let us now divide **M** in eq 17 into two parts

$$\mathbf{M} = \mathbf{M}^{(0)} + \epsilon\mathbf{M}^{(1)} \qquad (0 \leq \epsilon \leq 1) \quad \text{(G1)}$$

where $\mathbf{M}^{(0)}$ consists of only the diagonal elements of **M**, and $\mathbf{M}^{(1)}$ consists of only the off-diagonal elements of **M**, and ϵ is a parameter which is set to unity eventually. Putting the eigenvalue and column eigenvector of **M** to be $\lambda_p = \lambda_p{}^{(0)} + \epsilon\lambda_p{}^{(1)} + \ldots$ and $\mathbf{U}_p = \mathbf{U}_p{}^{(0)} + \epsilon\mathbf{U}_p{}^{(1)} + \ldots$, respectively, we have immediately

$$\lambda_p{}^{(0)} = p(p + 1) + \mu^2L_0(p) \quad \text{(G2a)}$$

$$\mathbf{U}_p{}^{(0)} = (0, \ldots, 0, 1, 0, \ldots, 0)^{\mathrm{T}} \quad \text{(G2b)}$$

Let us define $H_{kp} = [\mathbf{U}_k{}^{(0)}]^{\mathrm{T}}\mathbf{M}^{(1)}\mathbf{U}_p{}^{(0)}$. Then, we have only four kinds of H_{kp}'s:

$$H_{p,p-2} = \mu^2L_1(p) \qquad H_{p,p+2} = \mu^2L_2(p)$$
$$H_{p-2,p} = \mu^2L_2(p-2) \qquad H_{p+2,p} = \mu^2L_1(p+2) \quad \text{(G3)}$$

Due to this fact, a standard perturbation technique[31] gives a very simple result. We have

$$\lambda_p{}^{(1)} = 0 \quad \text{(G4a)}$$

$$\mathbf{U}_p{}^{(1)} = (0, \ldots, 0, a_p(p-2), 0, a_p(p+2), 0, \ldots, 0)^{\mathrm{T}} \quad \text{(G4b)}$$

with

$$a_p(p-2) = \frac{\mu^2L_2(p-2)}{\lambda_p - \lambda_{p-2}}$$
$$a_p(p+2) = \frac{\mu^2L_1(p+2)}{\lambda_p - \lambda_{p+2}} \quad \text{(G5)}$$

where the superscript (0) is omitted in λ because $\lambda_p = \lambda_p{}^{(0)}$ is to the first order in ϵ. The line eigenvector is similarly obtained ($\epsilon = 1$)

$$\mathbf{U}_p{}^* = (0, \ldots, 0, a_p{}^*(p-2), 1, a_p{}^*(p+2), 0, \ldots, 0) \quad \text{(G6)}$$

with

$$a_p{}^*(p-2) = \frac{\mu^2L_1(p)}{\lambda_p - \lambda_{p-2}} \qquad a_p{}^*(p+2) = \frac{\mu^2L_2(p)}{\lambda_p - \lambda_{p+2}} \quad \text{(G7)}$$

Substituting these results into eq 24b, we have to the first order in ϵ ($\epsilon = 1$)

$$G^1(\tau) = G_D(\tau)\sum_{\text{even } n}\left[(2n+1)b_n(k)^2e^{-\lambda_n\Theta\tau} - 2(2n+5) \times b_n(k)b_{n+2}(k)\mu^2L_2(n)\frac{e^{-\lambda_n\Theta\tau} - e^{-\lambda_{n+2}\Theta\tau}}{\lambda_n - \lambda_{n+2}}\right] \quad \text{(G8)}$$

If we take account of the differences in definition of various quantities, we find that eq G8 is exactly the same as the previous one[15] which is to order μ^2. [Equation 17 in ref 15 has typographical errors. It should read $a_0(ql) = b_0{}^2 + (1/15)D'(ql)^2b_0b_2 + \ldots$ and $a_2(ql) = (1/5)b_2{}^2 - (1/15) \times D'(ql)^2b_0b_2 + \ldots$]. Expanding all the factors containing μ^2 into power series of μ^2 and retaining terms up to μ^2 in the resultant equation, we have from eq G8

$$G^1(\tau) = G_D(\tau)\sum_{\text{even } n}\left[(2n+1)b_n(k)^2[1 - \mu^2L_0(n)\Theta\tau]e^{-n(n+1)\Theta\tau} - 2(2n+5) \times b_n(k)b_{n+2}(k)\mu^2L_2(n)\frac{e^{-n(n+1)\Theta\tau} - e^{-(n+2)(n+3)\Theta\tau}}{n(n+1) - (n+2)(n+3)}\right] \quad \text{(G9)}$$

Equation G9 is exactly the same as the previous ones,[13,14] although the apparent expression is slightly different from them because of differences in definition of various quantities.

A single time-scale analysis[13,14] results in a power series expression in $\mu^2\tau$ as the factor $[1 - \mu^2L_0(n)\Theta\tau]$ in eq G9. Due to this factor, eq G9 fails to hold for longer times. A multiple time-scale analysis can avoid this difficulty to order ϵ^4 (which corresponds to our ϵ^2 or μ^4).[15] We adopted a perturbation technique not to solve eq 16 but to solve eq 17 (or to diagonalize **M**). In our solution (eq 18), time appears only in the exponential factors, although the single time-scale analysis was applied to order μ^2. Needless to say, the first cumulant derived from eq G8 and G9 is the same as that in eq 29, because the perturbation result is expressed as functions of τ and $\mu^2\tau$, which is valid at very short times irrespective of μ^2 values.

The time behavior of the $n = 0$ mode in eq G8 is given by $\exp(-DK^2\tau)$ irrespective of μ^2 values. This inadequate behavior is greatly decreased if λ_0 of the first 3×3 portion of **M** is used. If we use λ_n ($n = 0$, 2, and 4) of the 3×3 matrix, eq G8 gives precise $G^1(\tau)$ for μ^2 up to 7. The famous formula for roots of $y^3 + ay + b = 0$ can be used to find λ_n's.

In a brief summary in ref 32, we noticed the clever method of Gierke[33] which many previous authors[15,16,19] cited but we could never consult before. We discuss here the relationship between his theory and ours in our own version. By use of the prolate spheroidal wave functions $\psi_p(\mu,\xi)$ which satisfies

$$[-\nabla_\xi{}^2 + \mu^2\xi^2]\psi_p(\mu,\xi) = \lambda_p\psi_p(\mu,\xi) \quad \text{(G10)}$$

$$\psi_p(\mu,\xi) = \sum_{n\geq 0}A_{p,n}P_n(\xi) \quad \text{(G11)}$$

the Green function is written as (cf. eq 20b and 22)

$$g_K^{\mu}(\xi,\xi';\tau) = \sum_p (1/N_p)\psi_p(\mu,\xi)\psi_p(\mu,\xi')e^{-\lambda_p\Theta\tau}$$

$$= \sum_p \sum_n \sum_l (1/N_p)A_{p,n}A_{p,l}P_n(\xi)P_l(\xi')e^{-\lambda_p\Theta\tau} \quad \text{(G12)}$$

where N_p is the normalization constant. From eq G12, we immediately have the apparently similar result to eq 24b:

$$G^1(\tau) = G_D(\tau)\sum_p \sum_n \sum_l (1/N_p)e^{-\lambda_p\Theta\tau}A_{p,n}A_{p,l}(i)^n(-i)^l b_n(k)b_l(k) \quad \text{(G13)}$$

Equation G13 is Gierke's result. His theory is mathematically equivalent to ours, because eq G10, G11, and A2 give the recurrence formula for $A_{p,n}$ which has the same form as that for $U_p(n)$ derived from substitution of eq 19b into eq 12. Both λ_p and $A_{p,n}$ can be computed one by one by use of formulas for spheroidal wave functions.[34] We computed the necessary number of λ_p and $U_p(n)$ at once by the matrix method. Gierke's theory is superior to any other theories in the sense that it can give an exact analytical expression of $G^1(\tau)$ for relatively small μ^2 values. In machine computation of $G^1(\tau)$ for large μ^2 (or $\bar{\mu}^2$) values, Gierke's method and ours will require almost the same amount of task. If subroutines for matrix calculations are available, our method provides a very simple way.

References and Notes

(1) Fujime, S. *J. Phys. Soc. Jpn.* **1970**, *29*, 751.
(2) Fujime, S.; Ishiwata, S. *J. Mol. Biol.* **1971**, *62*, 251.
(3) Ishiwata, S.; Fujime, S. *J. Mol. Biol.* **1972**, *68*, 511.
(4) Carlson, F. D.; Fraser, A. B. *J. Mol. Biol.* **1974**, *89*, 273.
(5) Fraser, A. B.; Eisenberg, E.; Kielley, W. W.; Carlson, F. D. *Biochemistry* **1975**, *14*, 2207.
(6) Maeda, T.; Fujime, S. *J. Phys. Soc. Jpn.* **1977**, *42*, 1983.
(7) Hochberg, A.; Low, W.; Tirosh, R.; Borejdo, J.; Oplatka, A. *Biochim. Biophys. Acta* **1977**, *460*, 308.
(8) Fujime, S.; Maruyama, M.; Asakura, S. *J. Mol. Biol.* **1972**, *68*, 347.
(9) Loh, E.; Ralston, E.; Schumaker, V. N. *Biopolymers* **1979**, *18*, 2549.
(10) Newman, J.; Carlson, F. D. *Biophys. J.* **1980**, *29*, 37.
(11) Gethner, J. S.; Gaskin, F. *Biophys. J.* **1978**, *24*, 505.
(12) Kubota, K.; Chu, B.; Fan, S.-F.; Dewey, M. M.; Brink, P.; Colflesh, D. E. *J. Mol. Biol.* **1983**, *166*, 329.
(13) Maeda, H.; Saito, N. *J. Phys. Soc. Jpn.* **1969**, *27*, 984.
(14) Schaefer, W. D.; Benedek, G. B.; Schofield, P.; Bradford, E. *J. Chem. Phys.* **1971**, *55*, 3884.
(15) Rallison, J. M.; Leal, L. G. *J. Chem. Phys.* **1981**, *74*, 4819.
(16) Wilcoxon, J.; Schurr, J. M. *Biopolymers* **1983**, *22*, 849.
(17) Doi, M.; Edwards, S. F. *J. Chem. Soc., Faraday Trans. 2* **1978**, *74*, 560.
(18) (a) Maguire, J. F.; McTague, J. P.; Rondelez, F. *Phys. Rev. Lett.* **1980**, *45*, 1891; *Ibid.* **1981**, *47*, 148. (b) Maguire, J. F. *J. Chem. Soc., Faraday Trans. 2* **1981**, *77*, 513.
(19) Zero, K. M.; Pecora, R. *Macromolecules* **1982**, *15*, 87.
(20) Maeda, T.; Fujime, S. *Macromolecules* **1981**, *14*, 809.
(21) Fujime, S.; Maeda, T.; Ishiwata, S. "Biomedical Applications of Laser Light Scattering"; Sattelle, D. S. et al., Eds.; Elsevier Biomedical Press: Amsterdam, 1982; p 251.
(22) Due to this definition of **M**, all vectors and matrices appearing in the text have sizes $((N/2) + 1)$ and $((N/2) + 1)^2$, respectively. However, subscripts specifying their elements are taken to be even integers. For examples, A_4 and $B_{0,6}$ should read the 2nd element of a vector **A** and the 3rd element of the 0th line of the matrix **B**, respectively.
(23) Fujime, S. *Macromolecules* **1973**, *6*, 361, where $U_p(n)U_p(l)$ in eq 56a should read $U_p(n)U_p^*(l)$.
(24) Pecora, R. *J. Chem. Phys.* **1968**, *48*, 4126.
(25) Doi, M. *J. Phys. (Orsay, Fr.)* **1975**, *36*, 607.
(26) Mori, Y.; Ookubo, N.; Hayakawa, R.; Wada, Y. *J. Polym. Sci., Phys.* **1982**, *20*, 2111.
(27) Fujime, S. *J. Phys. Soc. Jpn.* **1971**, *31*, 1805.
(28) Fujime, S.; Kubota, K. *Macromolecules* **1984**, *17*, 441.
(29) Smith, B. T.; Boyle, J. M.; Dongarra, J. J.; Barbow, B. S.; Ikebe, Y.; Clema, C. V.; Molar, C. B. Matrix Eigensystem Routines—EISPAK Guide, "Lecture Notes in Computer Science", 2nd ed.; Springer-Verlag: New York, Heidelberg, Berlin, 1976; p 48.
(30) Genz, A. C.; Malik, A. A. *J. Comp. Appli. Math.* **1980**, *6*, 295.
(31) Schiff, L. I. "Quantum Mechanics", 2nd ed.; McGraw-Hill: New York, Toronto, London, 1955.
(32) Loh, E. *Biopolymers* **1979**, *18*, 2569.
(33) Gierke, T. D. Ph.D. Thesis, University of Illinois, 1973.
(34) Lowan, A. N. in "Handbook of Mathematical Functions with Formulas, Graphs, and Mathematical Tables"; Abramowitz, M.; Stegun, I. A.; Eds.; Dover Publications: New York, 1970; p 752.
(35) An experimental test of our theory is in: Kubota, K.; Urabe, H.; Tominaga, Y.; Fujime, S. *Macromolecules*, in press. An extension of the present theory to semiflexible filaments is in: Maeda, T.; Fujime, S. *Macromolecules*, in press.

Absorption Spectrum of the Triplet State and the Dynamics of Intramolecular Motion of Polystyrene

Seiichi Tagawa*

Research Center for Nuclear Science and Technology, University of Tokyo and Nuclear Engineering Research Laboratory, Faculty of Engineering, University of Tokyo, Tokai-mura, Ibaraki, 319-11, Japan

Nobuaki Nakashima and Keitaro Yoshihara

Institute for Molecular Science, Myodiji, Okazaki, 444, Japan.

Received July 7, 1983

ABSTRACT: Transient absorption spectra in the wavelength range between 220 and 900 nm have been measured in the KrF excimer laser (248 nm) photolysis of polystyrene in cyclohexane solutions. Although the absorption spectrum with the shoulder around 300–350 nm and a small tail around 400 nm had been correlated to the triplet state of polystyrene,[1] the $T_n \leftarrow T_1$ absorption spectrum of polystyrene with a single peak at 230 nm, two shoulders around 250–270 and 300–350 nm, and a small tail in the wavelength region longer than $\lambda = 400$ nm is identified clearly in the present work, in addition to the excimer absorption band at 520 nm with a lifetime of 20 ns, which had been reported previously by us.[1,2] The lifetime of the triplet state of polystyrene is 110 ns and is a clue to the internal rotation of polystyrene, because the lifetime of the triplet state of polystyrene is determined by self-quenching on the basis of intramolecular interaction between triplet- and ground-state chromophores. Comparison of the present results with literature values for internal rotation, measured by other techniques, is also presented.

Introduction

A number of papers have been published on photoinduced[3] and radiation-induced[4] reactions of polystyrene, because it is the simplest polymer with aromatic chromophores and photoinduced and radiation-induced main-chain cleavage of polystyrene is very important in

0024-9297/84/2217-1167$01.50/0